Acoustophoretic Volumetric Displays using a Fast-Moving Levitated Particle

Tatsuki Fushimi[1], Asier Marzo[2], Bruce W. Drinkwater[1], Thomas L. Hill[1]

1) Department of Mechanical Engineering, University of Bristol, BS8 1TR, Bristol, United Kingdom

2) UpnaLab, Universidad Pública de Navarra, Pamplona 31006, Navarre, Spain

Supplementary Material

Experimental Setup for Particle Tracking

FIG. S1 (a) shows the experimental setup, and FIG. S1 (b) shows an image of a typical EPS particle used in the acoustic levitator, as seen by the camera.

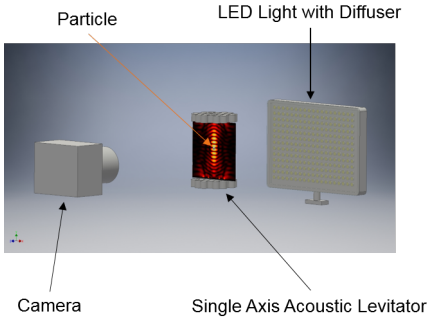

(a) Experimental Setup for particle tracking

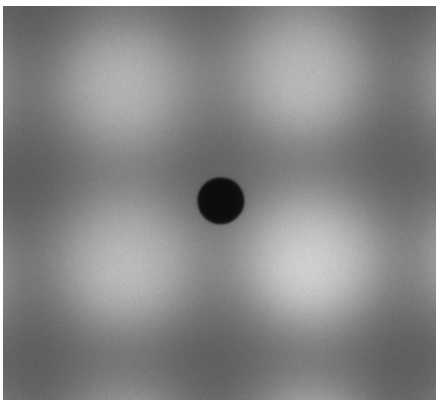

(b) Typical EPS particle levitated in the acoustic levitator

FIG. S1: Experimental Setup and EPS Particle

Calculation of Phase Delay for focusing on a point

To move a particle to a specific point, the phase delays between the waves emitted from each transducer need to be calculated in order to focus at the target point ($\boldsymbol{x_f} = (x_f, y_f, z_f)$). The required phase delays are calculated by:

$$\phi_{focal,n} = -\frac{2\pi f_0}{c_0}\left(|\boldsymbol{x}_{t,n} - \boldsymbol{x_f}| - |\boldsymbol{x_f}|\right) + \phi_{t,n} \tag{S1}$$

where $\boldsymbol{x}_{t,n}$ is the transducer position (x_t, y_t, z_t), $\phi_{t,n}$ is the phase shift needed to create an anti-node at the focal point, i.e. $\phi_t = 0$ for lower phased-array and $\phi_t = \pi$ for the upper phased-array, this shifts the nodes to the anti-nodes such that particles get trapped at the target point. The levitator is made of 2 opposed arrays of 30 transducers each arranged as shown in FIG.S2. The arrays faced each other to create a single-axis acoustic levitator.

Simulation of Static Equilibrium Points

Assuming that the particle is small ($r = 0.657\,\text{mm}$, $m = 0.050\,\text{mg}$) in comparison to the wavelength ($\lambda = 8.6\,\text{mm}$), the acoustic radiation force is calculated using Gor'kov's potential [1]:

$$F^{rad} = -\nabla U^{rad} \tag{S2}$$

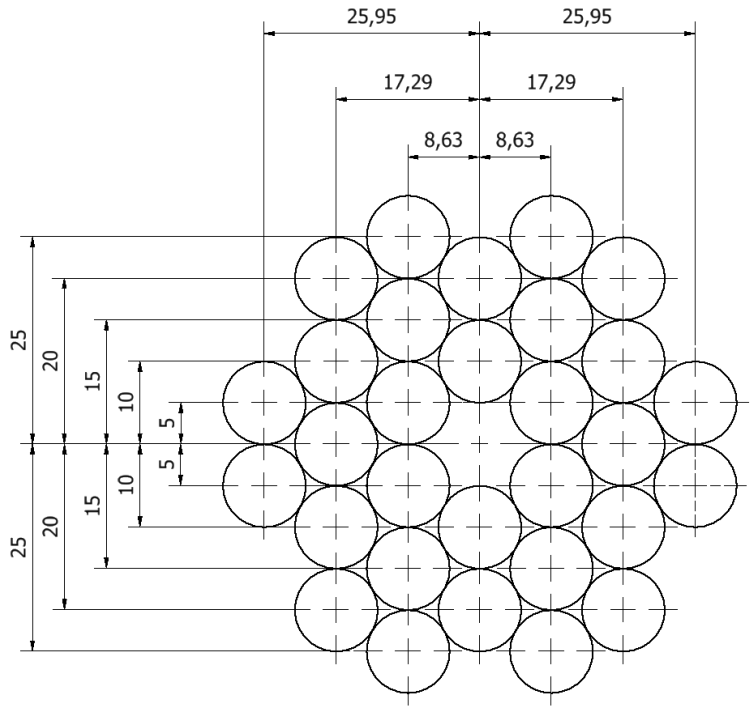

FIG. S2: Transducer Positions in the Acoustic Levitator

$$U^{rad} = \frac{4\pi}{3} r^3 \left[\frac{f_1 \kappa_0 \langle p_{in}^2 \rangle}{2} - \frac{3 f_2 \rho_0 \langle v_{in}^2 \rangle}{4} \right] \tag{S3}$$

where $f_1 = 1 - \frac{\kappa_p}{\kappa_0}$, $f_2 = \frac{2(\tilde{\rho}-1)}{2\tilde{\rho}+1}$, and $\tilde{\rho} = \frac{\rho_p}{\rho_0}$. ρ is density, $\kappa = \frac{1}{\rho c}$ is compressibility, p_{in} and v_{in} are incident pressure and velocity fields, respectively. Subscript 0 represents the properties of the fluid medium and p of the particle. The temperature, barometric pressure and humidity were recorded at the beginning of the experiment, and at 19.1°C, the values of air density (ρ_a), viscosity (μ) and speed of sound (c_0) were $1.20\,\mathrm{kg\,m^{-3}}$, $1.81 \times 10^{-5}\,\mathrm{kg\,(m\,s)^{-1}}$, and $343.2\,\mathrm{m\,s^{-1}}$, respectively. The pressure field (p_{in}) generated by the setup was calculated using Huygens' principle:

$$p_{in} = \sum_{n=1}^{60} \frac{P_0 D_f(\theta)}{d_n} \mathrm{e}^{\mathrm{j}(\phi_{focal,n} + k d_n)} \tag{S4}$$

where $D_f(\theta) = |\frac{2J_1(v)}{v}|$ is the far-field directivity function for a piston source where J_1 is the Bessel function of the first kind of order 1, $v = ka\sin(\theta)$ where the transducer radius $a = 0.0045$ m. $P_0 = 1.555$ Pa at one meter when the transducer is driven at 9 V (the levitator was operated at this voltage unless otherwise stated), and $d_n = |\boldsymbol{x}_{t,n} - \boldsymbol{x}|$. The equilibrium point of a particle in simulation is determined by balancing the acoustic radiation force from equation S2 and the gravity force ($F_{grav} = mg$).

Static Trajectory Calibration

A static calibration approach was applied to the trajectories associated with FIG. 2 and 3 using the method described in Fushimi et al. [2]. A particle was moved in a raster fashion over the plane(s) of interest while camera(s) were used to record the location of the particle (note that in the case of 2 cameras they were located orthogonally). FIG. S3 shows the deviation between the simulated and the experimental

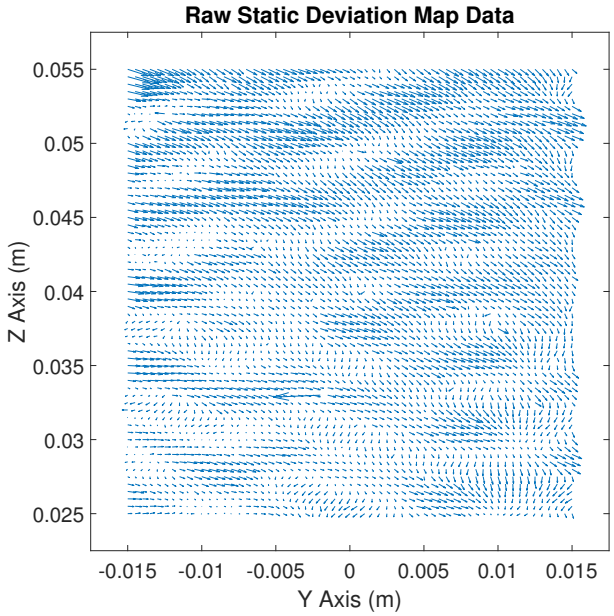

FIG. S3: Quiver plot showing the deviation of the equilibrium point from the focal point

equilibrium points. The calibration process then uses this information to find the optimal sets of focal points that achieve the target trajectory.

As the particle radius is relatively large in comparison to the width of the image, subpixelation was employed to enhance the image quality of the rendered image as shown in FIG. S4. Subpixelation was achieved by layering extra sets of rows and columns between the raster graphics generated for the non-subpixelated images, and the color was adjusted such that when summed together, generates the RGB code as specified by the original image.

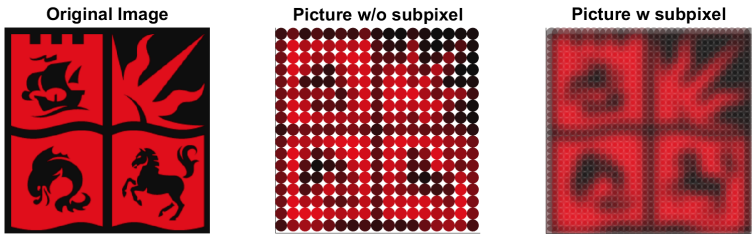

FIG. S4: Image Enhancement by Subpixelation of Images

For the 3D volumetric image in FIG. 2 (d)-(f) the target trajectory is as shown in FIG. S5 (a)-(c). Newton's

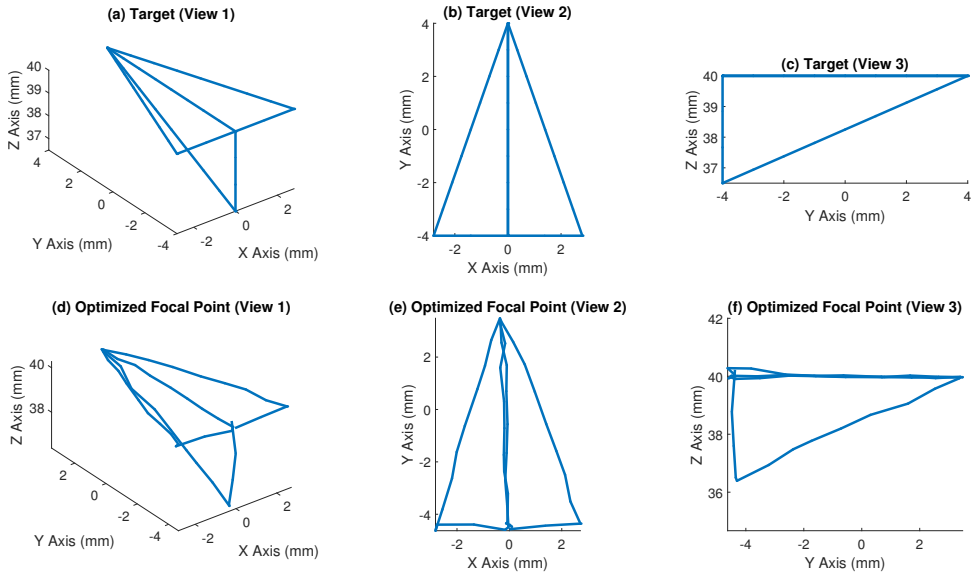

FIG. S5: Wireframe Plane Trajectory

method was utilized for the 3D calibration:

$$u = \bar{u} + \hat{u} \tag{S5}$$

where u is the desired solution, $\bar{u}$ is the guess and $\hat{u}$ is the correction term.

$$f(\bar{u}+\hat{u}) = f(\bar{u}) + f'(\bar{u})(T-\hat{u}) \tag{S6}$$

where f is the equilibrium point function of focal points u, and T is the target equilibrium point. The correction factor is then:

$$\hat{u} = -[f'(\bar{u})]^{-1}(T - f(\bar{u})) \tag{S7}$$

As the u is a 1x3 vector, $f'(\bar{u})$ is a Jacobian:

$$J = \begin{pmatrix} \frac{\delta x}{\delta u_1} & \frac{\delta x}{\delta u_2} & \frac{\delta x}{\delta u_3} \\ \frac{\delta y}{\delta u_1} & \frac{\delta y}{\delta u_2} & \frac{\delta y}{\delta u_3} \\ \frac{\delta z}{\delta u_1} & \frac{\delta z}{\delta u_2} & \frac{\delta z}{\delta u_3} \end{pmatrix} \tag{S8}$$

The gradient $\frac{\delta X}{\delta U}$ was determined by experimentally perturbing the focal point by a small increment, h:

$$\frac{\delta X}{\delta U} = \frac{f(X+h) - f(X-h)}{2h} \tag{S9}$$

If the correction factor is > 0.5 mm then a damping factor of 0.5 was applied to prevent overshooting. The resultant calibrated trajectory is as shown in FIG. 2 (d)-(f).

Procedure for Recording the Volumetric Display

All photographic images in the paper are recorded using a DSLR camera (Nikon D610) on a tripod, parallel to the plane of the axis of the volumetric image. Fixed shutter speed was employed for both FIG. 2 and 3. The exposure time is 20 seconds for FIG. 2 (a)-(c), and 5 seconds for (d)-(f). The recorded

images are stored as JPG files, and no digital enhancement has been applied to the images apart from cropping for FIG. 2. The dimensions for the wireframe plane in FIG. 2 (d)-(f) are in the aforementioned FIG. S5, the image size for FIG. 2 (a)-(c) is 23.1 by 23.1 mm. Digital enhancement (function 'imadjustn' in MATLAB Image Processing Toolbox) and cropping has been applied to images in FIG. 3 to increase the visibility of the particle trajectory.

Data Processing of the Dynamic Response

The recorded footage of the oscillation response was processed using MATLAB's Image Processing Toolbox. The camera was calibrated using a CMM stylus (Renishaw A-5000-7806) with a custom made holder that places the center of the ruby ball at 0.04 m from the base of holder, and the pixel to mm ($3.23 \times 10^{-5}\,\mathrm{m\,pix^{-1}}$) conversion rate and Y and Z axis datum points were identified. The Y and Z position of the particle was identified using Hough Circle Transform, and the position signal was then processed using DFT. The principal component of the DFT was used to identify the amplitude and the frequency of the oscillation.

Light Intensity Measurement of Particle

The light intensity of the particle was measured using the DSLR camera (Nikon D610). The location of LED light source was fixed, and pictures were taken from front, side, and back with approximately the same distance, as shown in FIG. S6. The RGB color values at the centre of the particle was extracted, and light intensity was calculated by:

$$I = \frac{1}{3}(R+G+B) \tag{S10}$$

The measured light intensity was 128, 91, and 61 for front, side and back, respectively. This is a reduction of the light intensity by 71.5 % and 48.0 % for "front to side" and "front to back", respectively.

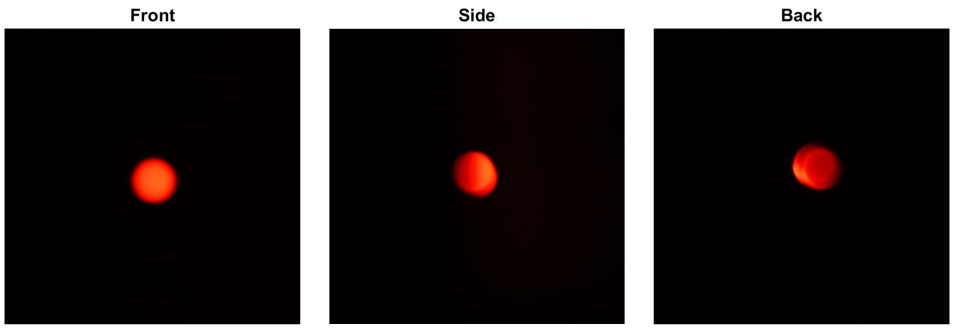

FIG. S6: Light Intensity as Observed from Different Angles

Dynamic Response of the Particle inside the Acoustic Levitator

To model the dynamic response of the particle, the force was balanced between acoustic radiation force, inertia, damping force (F_{drag}) and gravity (F_{grav}):

$$\begin{pmatrix} m\ddot{y} \\ m\ddot{z} \end{pmatrix} = \begin{pmatrix} F_{rad,y} + F_{drag,y} \\ F_{rad,z} + F_{drag,z} + F_{grav} \end{pmatrix} \tag{S11}$$

In order to increase the computational efficiency of the ordinary differential equation solver, the acoustic radiation force was fitted with the polynomial function of form:

$$F_{rad} = fn(y,z,f_y,f_z) = \sum_{n=0}^{N} \alpha_n (y - y_{off})^{A_{1,n}} (z - z_{off})^{A_{2,n}} (f_z - f_{z,off})^{A_{3,n}} \tag{S12}$$

where A is every combination of polynomial orders for 3 variables from 0 to 13 for y and z axis and 0 to 12 for f_z. A has a size of 559 by 3, and therefore there are 559 α_n coefficients. y_{off} and z_{off} were normalizing constants and they were 0 and 0.04, respectively. The coefficients are found by matrix operation:

$$\alpha_n = \left[y^{A_{1,n}} z^{A_{2,n}} f_z^{A_{3,n}} \right]^{-1} F_{rad} \tag{S13}$$

The focal points are discretized by 1000 steps for each amplitude, and the coordinates are limited by windowing ± 2 mm and ± 3.5 mm for y and z respectively, around the focal point. For this step of the calculation, a large memory node of high computational capabilities at the University of Bristol was used for the calculation.

The drag force was calculated by:

$$F_d = C_d \frac{\pi}{4} d^2 \frac{1}{2} \rho u^2 \tag{S14}$$

where d is the diameter of the particle and u is velocity. Coefficient of drag is approximated by using Flemmer & Banks [3]:

$$C_d = \frac{24}{Re} 10^E \tag{S15}$$

where $E = 0.261\mathrm{Re}^{0.369} - 0.105\mathrm{Re}^{0.431} - \frac{0.124}{1+log(\mathrm{Re})^2}$ and it is applicable for $Re < 3 \times 10^5$. Equation S11 was solved using VSVO solver (ode15s) on MATLAB, as high tolerances were required for Runge-Kutta (ode45) solver. The dynamic response of the acoustic levitator was solved using a combination of Huygens' principle and Gor'kov's method (see section on Calculation of Equilibrium Point) is as shown in FIG S7.

Hybrid Model

The hybrid model incorporates the equilibrium position information from the experiment into the Gor'kov's numerical model of the acoustic radiation forces. Firstly, the equilibrium point in the numerical model is identified by the aforementioned methods. Then, the difference between the numerically found equilibrium point and experimentally obtained equilibrium point is taken:

$$\mathbf{x}_{delta} = \mathbf{x}_{eq,sim}(f_z) - \mathbf{x}_{eq,exp}(f_z) \tag{S16}$$

The required force field is the translated version of equation S12:

$$F_{rad} = \sum_{n=0}^{N} \alpha_n (y - (y_{off} + y_{delta}(f_z)))^{A_{1,n}} (z - (z_{off} + z_{delta}(f_z)))^{A_{2,n}} (f_z - f_{z,off})^{A_{3,n}} \tag{S17}$$

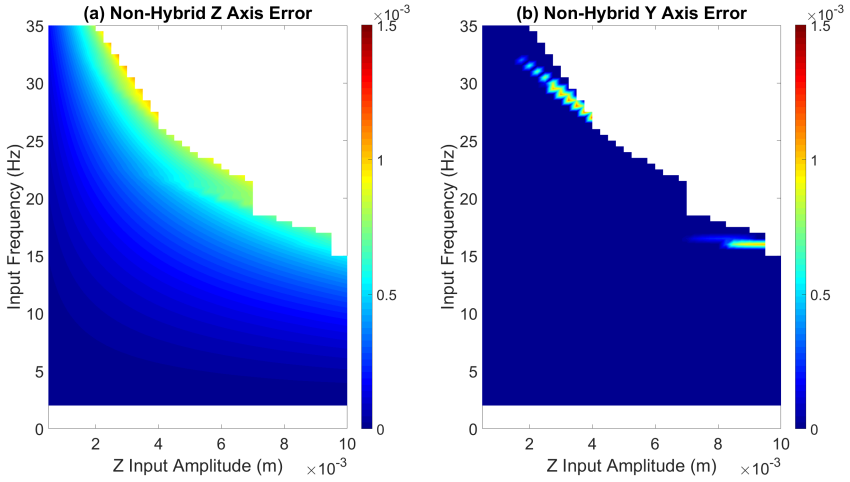

FIG. S7: Simulation of the Dynamic Response using a Huygens' Model and the Gor'kov acoustic radiation force model

Effects of Increasing Voltage on the Dynamic Response

Similarly to the experimental measurement of the dynamic response, the particle was oscillated vertically with amplitude in the range of $0.5\,\text{mm} \leq A \leq 8\,\text{mm}$. In contrast to the experimental approach, we use a sine-sweep rather than stepped-sine excitation, with an aim to determine the frequency at which the particle is ejected from the levitator, and the result is as shown in FIG. S8.

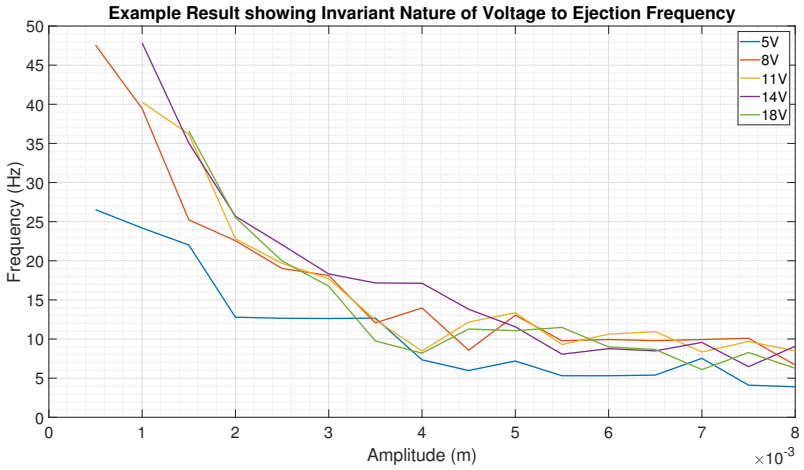

FIG. S8: Particle ejection limits for different applied voltages showing that voltage does not significantly affect the ejection frequency of the particle. The experiment for each amplitude starts as a low frequency of oscillation and proceeds until the particle is ejected.

Reproducibility Study of Ejection Frequency

The consistency of the ejection frequency was evaluated for the levitator, and an example of such results are as shown in Table. S1.

Amplitude (mm)	Expt. 1 (Hz)	Expt. 2 (Hz)	Expt. 3 (Hz)	Mean (Hz)	Standard Deviation
1.0	35.3	42.1	37.7	38.4	3.44
1.5	28.6	30.6	33.0	30.7	2.23
2.0	20.3	24.8	22.1	22.4	2.25
2.5	15.3	19.4	21.0	18.6	2.92
3.0	14.3	13.0	15.5	14.3	1.24
3.5	10.0	9.8	13.0	10.9	1.79
4.0	12.2	12.5	11.9	12.2	0.32
4.5	10.4	12.2	8.71	10.4	1.77
5.0	10.2	10.1	13.4	11.2	1.89
5.5	8.09	9.17	9.18	8.81	0.62
6.0	7.91	9.17	7.61	8.23	0.83

Table S1: Example showing the variability of the ejection frequency of particle from the acoustic trap

Transducer Response to Rapidly Varying Phase

A transducer that was used in the experiment was taken off from the array, and its acoustic response was recorded using B&K Microphone (4138-A-015) connected to a ADC (Handyscope HS3). The pressure microphone was placed 15 mm from the surface of the transducer in a free-space environment. The transducer was excited using the FPGA board used in the experiment at varying degrees of phase velocity. This was achieved by sending signals to the transducer that would have been sent for the statically calibrated trajectory of a circle with a radius, $r = 0.004742\,\mathrm{m}$. The circle's update frequency was increased gradually from $\approx 1.5, 8.0$ to $14.8\,\mathrm{Hz}$. FIG. S9 shows an example response of the transducer. As the velocity of particle increases, the demanded value of phase changes more rapidly in comparison to when the particle was moving slowly. As a result, it causes the acoustic pressure field generated by the transducer to drop significantly.

Transducer Modelling and Wider Bandwidth Transducer

The simplest approximation of the acoustic transducer is to model it as a single DoF linear mass-spring-damper oscillator:

$$\ddot{x} + \frac{\omega_n}{Q}\dot{x} + \omega_n^2 x = F(t) \tag{S18}$$

where ω_n is the natural frequency, $Q = \frac{1}{2\zeta}$ is the quality factor Q in acoustic terms. Using a similar apparatus as the previous section, the acoustic Q factor of the transducer was measured experimentally using pressure microphone. A function generator (Agilent 3320A) was connected to the transducer instead of the FPGA board to generate a sinusoidal signal in the range of 35000 Hz to 45000 Hz with the

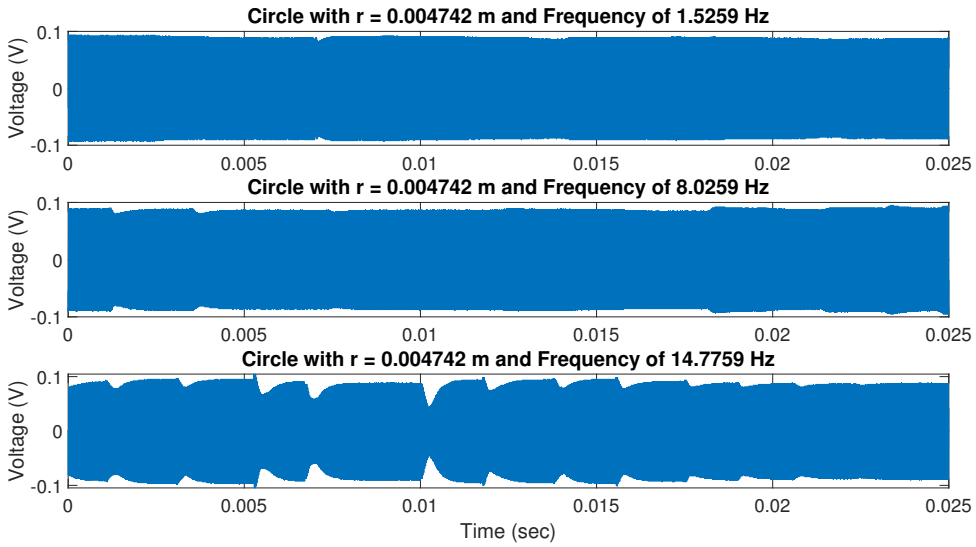

FIG. S9: Time domain response (received voltage is proportion to acoustic pressure) for different rates of change of phase.

increment of 100 Hz. The Q factor calculated from:

$$Q = \frac{\omega_n}{\Delta\omega_{3dB}} \tag{S19}$$

where ω_{3dB} is the 3dB bandwidth of the acoustic pressure response. For a Murata transducer, ω_n and ω_{3dB} are 40200 and 3566.2 Hz, respectively. Thus, the Q factor for this transducer was 11.27. The transfer function for equation S18:

$$P(s) = \frac{1}{s^2 + \frac{\omega_0}{Q}s + \omega_n^2} \tag{S20}$$

In order to validate this transducer model, two signals (FPGA board signal to the transducer, and the acoustic transducer response measured 15 mm from the transducer) were recorded experimentally. The FPGA board signal was fed into the transfer function, P(s) and the comparison of the response is as shown in FIG. S10. Whilst the signal output is normalized and amplitude response match may be qualitative; the simple model of acoustic transducer captures the dynamic response of interest (i.e. off-resonance of the transducer). The transfer function's Q factor was now reduced to, for e.g. Q = 2, widening the bandwidth of the transducer. The same FPGA board signal in FIG. S10 was sent to the transfer function with lower Q factor, and the response is as shown in FIG. S11. Whilst there is still some observable amplitude fluctuation, the transducer more accurately recreates the desired output signal.

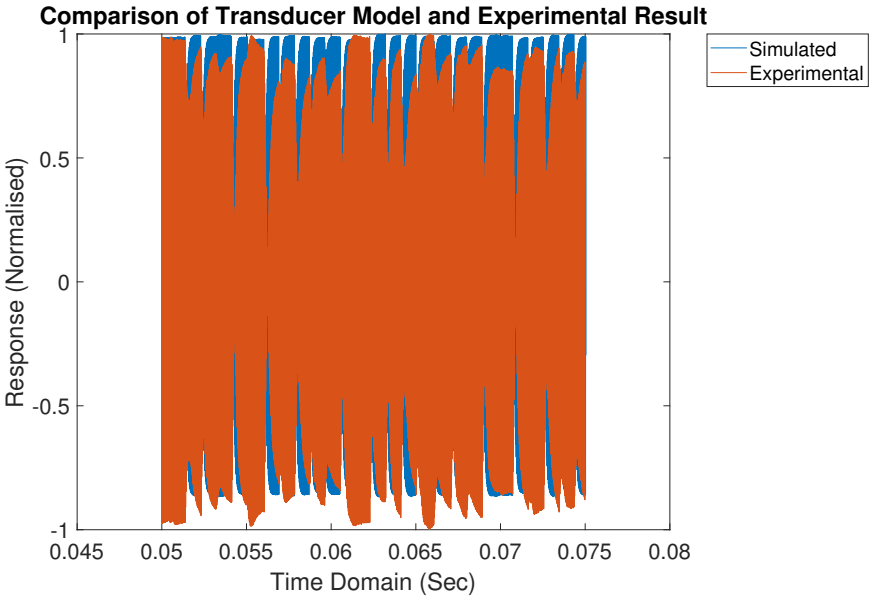

FIG. S10: Comparison of Transducer Model and Experimental Output

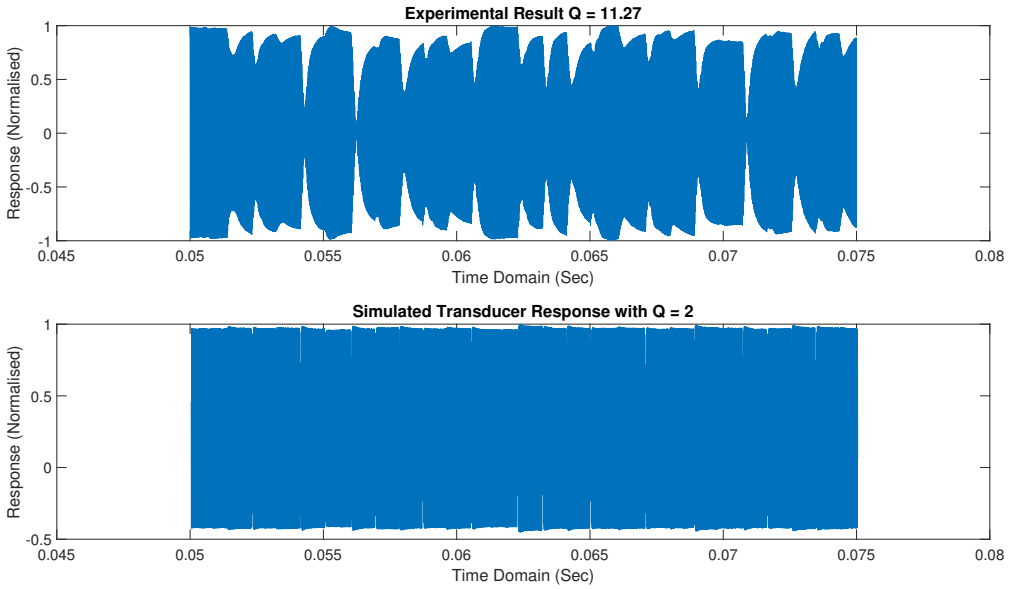

FIG. S11: Comparison of Experimental Result and Transducer with Wider Bandwidth

References

[1] L. P. Gor'kov. On the Forces Acting on a Small Particle in an Acoustical Field in an Ideal Fluid. *Soviet Physics Doklady*, 6:773, 1962.

[2] Tatsuki Fushimi, Asier Marzo, Thomas L Hill, and Bruce W Drinkwater. Trajectory Optimization of Levitated Particles in Mid-air Ultrasonic Standing Wave Levitators. *2018 IEEE International Ultrasonics Symposium (IUS)*, pages 1–9, 2018.

[3] R. L. C. Flemmer and C. L. Banks. On the drag coefficient of a sphere. *Powder Technology*, 48(3):217–221, nov 1986.